High-Confident Local Structure Guided Consensus Graph Learning For Incomplete Multi-view Clustering

Shuping Zhao[1], **Lunke Fei**[1], **Qi Lai**[2*], **Jie Wen**[3*], **Jinrong Cui**[4] and **Tingting Chai**[5]
[1]Guangdong University of Technology
[2]Shenzhen Institute of Advanced Technology, Chinese Academy of Sciences
[3]Harbin Institute of Technology, Shenzhen
[4]South China Agricultural University
[5] Harbin Institute of Technology
yb77458@um.edu.mo, flksxm@126.com, q.lai@siat.ac.cn, {wenjie,ttchai}@hit.edu.cn
tweety1028@163.com

Abstract

Current existing clustering methods for handling incomplete multi-view data primarily concentrate on learning a common representation or graph from the available views, while overlooking the latent information contained in the missing views and the imbalance of information among different views. Furthermore, instances with weak discriminative features usually degrading the precision of consistent representation or graph across all views. To address these probelms, in this paper, we propose a simple but efficient method, called high-confident local structure guided consensus graph learning for incomplete multi-view clustering (HLSCG_IMC). Specifically, this method can adaptively learn a strict block diagonal structure from the available samples using a block diagonal representation regularizer. Different from the existing methods using a simple pairwise affinity graph for structure construction, we consider the influence of instances located at the edge of two clusters on the construction of graph for each view. By harnessing the proposed high-confident strict block diagonal structures, the approach seeks to directly guide the learning of the robust consensus graph. A number of experiments have been conducted to verify the efficacy of our approach.

1 Introduction

Multi-view clustering (MVC) aims to categorize data points into their respective classes by comprehensively taking into account multiple feature representations, where each of these feature representations can be seen as a unique view [Sun *et al.*, 2024]. For instance, a webpage typically includes three types of representations, i.e., text, imagery, and hyperlinks. Besides this, the test results for a patient often contain different indicators, such as CT, blood routine, and electrocardiogram [Fu *et al.*, 2024] [Lyu *et al.*, 2024]. Given the prevalent occurrence of incomplete data, with missing views or instances, in practical applications such as recommendation systems, disease diagnosis, and multimedia analysis, the research of incomplete multi-view clustering (IMC) holds significant importance [Chen *et al.*, 2024] [Chao *et al.*, 2024]. Besides this, Khan et al. [Khan *et al.*, 2024] designed a weighted concept factorization approach.

Some common issues may emerge in the IMC tasks due to the absence of views [Wang *et al.*, 2022] [Wen *et al.*, 2021]: 1) The lack of views can complicate the integration of the remaining views, potentially reducing the accuracy and effectiveness of the clustering algorithm. 2) The problem of data imbalance caused by missing views makes the traditional multi-view clustering technique ineffective. Various researchers have undertaken considerable efforts to address these challenging IMC problems. For example, Cai et al. [Cai *et al.*, 2024] incorporates a completion term designed to fill in the missing samples in unbalanced incomplete multi-view clustering, which utilizes the inherent information contained within the absent views. Chao et al. [Chao *et al.*, 2024] introduces a multi-view consistency relation transfer combined with a graph convolutional network to address the missing values problem. This approach incorporates instance-level attention fusion and high-confidence guiding strategies to harness the complementary information available. Although existing IMC methods have achieved some positive performances, we notice that these approaches primarily focuses on pairwise-based geometric structures, which are easily affected by the weak feature expression or noisy [Gu *et al.*, 2024] [Wang *et al.*, 2023]. In particular, some samples located at the edge of two clusters are inaccurate in local structure learning due to their weak feature expression or noise effects. Therefore, accurate local structure learning is very important for calculating the affinity relationships between different samples [Yao *et al.*, 2024] [Zhong *et al.*, 2024].

Block diagonal structure (BDS) construction refers to the process of arranging a matrix into a block diagonal matrix form, where the matrix is partitioned into a series of smaller square submatrices along its main diagonal, and all elements outside these blocks are zero [Lu *et al.*, 2018]. The learning BDS means that samples of different categories are strictly differentiated, which makes intra-class samples show rela-

*indicates the co-corresponding authors

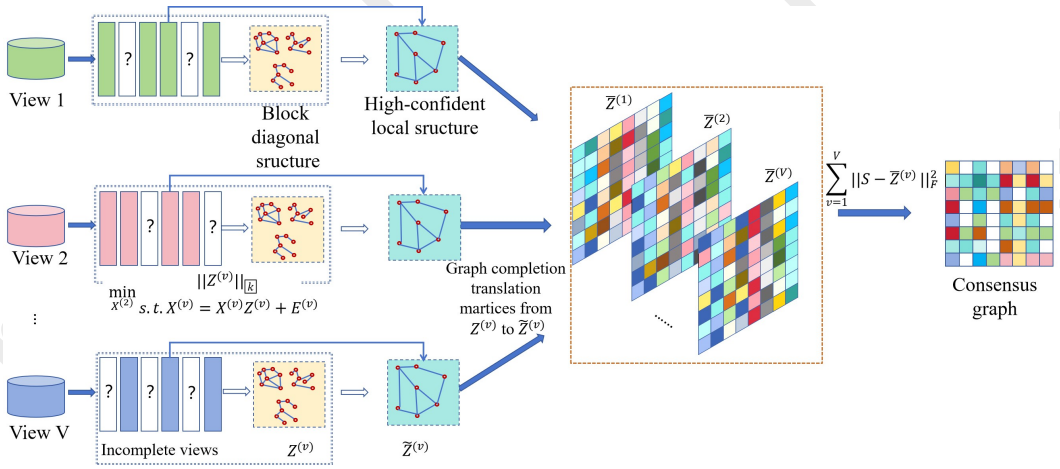

Figure 1: Some cases of multi-view data with different degrees of missing samples for each view.

tively high correlation [Zhuo *et al.*, 2024]. Consequently, the BDR is crucial in the incomplete multi-view learning, as it facilitates the model to accurately depict the internal connections of the available instances for each view [Liu *et al.*, 2023b]. This is essential in IMC tasks, since it can provide precise comprehensive and available information from different views for the derivation of complete structure.

Motivated by this observation, we propose a simple but efficient method, called high-confident local structure guided consensus graph learning for incomplete multi-view clustering (HLSCG_IMC). Specifically, this method can adaptively learn a strict block diagonal structure from the available samples using a block diagonal representation regularizer. Different from the existing methods using a simple pairwise affinity graph for structure construction, we consider the influence of instances located at the edge of two clusters on the construction of graph for each view. By harnessing the proposed high-confident strict block diagonal structures, the approach seeks to directly guide the learning of the robust consensus graph. As depicted in Fig.1, we first learn a high-confident local structure with a BDS regularizer for the available instances from each view. Afterwards, we reconstruct the complete graphs of all incomplete views by fully exploring the within-view and between-view information available in each view with the guiding of the learned high-confident local structure. Finally, unliking the existing consensus representation learning methods, we directly learn a confident affinity graph across all views for final clustering. Specifically, To ensure that the latent representation and graphs of all views achieve global optima, we integrate the high-confident local structure learning and the consensus graph completion into a unified joint optimization framework. The primary contributions of this paper are summarized as follows:

(1) Different from the other existing methods, we propose a high-confident local structure learning strategy, which considers the attribution of instances with weak feature representation located at the edge of two clusters.

(2) A HLSCG_IMC method is proposed, which can adaptively recover the complete graph for each view by exploiting the hidden information of missing instances and available instances to directly enhance the learning of consensus graph across all views.

(3) The proposed method can be flexibly applied to any types of IMC tasks. In addition, the experimental results proved the superiority of the proposed method in comparison with the other related methods.

2 Notations and Preliminaries

Given a matrix $A \in R^{m\times n}$, we define its l_F-norm and l_1-norm as $\| A \|_F^2 = \sum_{i=1}^{m}\sum_{j=1}^{n} a_{i,j}^2$ and $\| A \|_1 = \sum_{i=1}^{m}\sum_{j=1}^{n} |a_{i,j}|$, respectively, where $a_{i,j}$ presents the element on the (i,j)-th location. Additionally, The nuclear norm of matrix A is calculated as $\| A \|_* = \sum_i \gamma_i$, where γ_i indicates the ith singular value of A. The detailed notations of the used variables are presented in Table1.

Symbols	Description
$X^{(v)} \in R^{d_v\times n_v}$	The avaiable instances from the v-th view
$Z^{(v)} \in R^{n_v\times n_v}$	The graph of avaiable instances
V	The number of views
d_v	The dimensionality of instances
v	The v-th view
n_v	The number of instances from the v-th view
$W^{(v)} \in R^{n\times n}$	The affinity relationship matrix
$\bar{S}^{(v)} \in R^{n\times n}$	The complete graph for the v-th view
$S \in R^{n\times n}$	The consensus graph across all views
$E^{(v)} \in R^{d_v\times n_v}$	The learned noise of the available instances
$\tilde{Z}^{(v)} \in R^{n\times n}$	The high-confident graph
$F^{(v)} \in R^{n\times c}$	The consensus representaion across all views
c	The dimensionality of the consensus representation

Table 1: Description of the symbols used in this paper.

BDS: The block diagonal structure highlights the independence of the submatrices, enabling efficient storage and manipulation of the matrix, particularly in scenarios where the submatrices represent distinct or separable components of the

original matrix. By leveraging the sparsity and structural independence of the block diagonal matrix in (1), computations such as matrix multiplication, inversion, and eigenvalue analysis can be greatly simplified and accelerated. Here, we introduce two definitions abou BDR as follows [Lu *et al.*, 2018]:

Definition 1: Let $X = [X_1, X_2, ..., X_C] \in R^{d\times n}$ denote n training samples from C classes, where each column is a sample vector. Suppose that all the samples are rearranged based on the class labels, and each class of training samples are stacked together to form a sub-matrix $X_i \in R^{d\times n_i}$, which denotes n_i samples from the i-th class.

Definition 2: Given the data matrix $X = [X_1, X_2, ..., X_k]$ drawn from a union of k subspaces $\{S_i\}_{i=1}^k$, we say that Z obeys the Block Diagonal Property if Z is k-block diagonal, where the nonzero entries Z_i correspond to only X_i.

$$\begin{bmatrix} Z_1 & 0 & \cdots & 0 \\ 0 & Z_2 & \cdots & 0 \\ \vdots & \vdots & \ddots & \vdots \\ 0 & 0 & \cdots & Z_k \end{bmatrix} \tag{1}$$

Please note that the notions of the k-block diagonal matrix and the block diagonal property share certain connections as well as distinctions. The block diagonal property is tailored specifically for the context of subspace clustering problems, whereas the concept of a k-block diagonal matrix is more general and not confined to this particular application. A matrix that satisfies the block diagonal property is necessarily k-block diagonal, but the converse is not true. Additionally, the block diagonal property stipulates that each block must have a one-to-one correspondence with each data subject.

3 The Proposed Method

3.1 Learning Model

Various clustering methods based on graph learning have demonstrated that acquiring a high-quality graph, which unveils the underlying relationships within the data, is advantageous for achieving superior clustering performance [Liu *et al.*, 2023a][Zhou *et al.*, 2019]. Particularly, graph learning plays a pivotal role in multi-view clustering by enabling the extraction of intricate relationships and correlations between different views of the data. A block diagonal structure refers to a matrix that is partitioned into diagonal blocks, where each block is itself a square matrix, and all off-diagonal blocks are zero matrices. Furthermore, the block diagonal constraint can act as a regularizer, preventing the model from overly relying on any single view and encouraging it to discover shared and discriminative features across all views [Jiang *et al.*, 2025].

Given the multi-view dataset $X = \{X^{(v)}\}_{v=1}^V \in R^{d_v\times n}$, where v is the vth view, V presents the total number of views, and d_v denotes the dimensionality of the features from the vth view. Here, under the independent subspaces assumption, the self-representation matrix $Z^{(v)}$ for each view should be block diagonal as follows:

$$\begin{aligned} &\min_{Z^{(v)}} \sum_{v=1}^{V} \parallel X^{(v)} - X^{(v)}Z^{(v)} \parallel_F^2 + \gamma \parallel Z^{(v)} \parallel_{\boxed{k}} \\ &s.t.\ diag(Z^{(v)}) = 0,\ Z^{(v)} \geq 0,\ Z^{(v)} = {Z^{(v)}}^T \end{aligned} \tag{2}$$

where $||Z||_{\boxed{k}}$ is the block diagonal matrix structure induced regularizer. For the affinity matrix $Z^{(v)}$ on the vth view, its k-block diagonal regularizer $||Z^{(v)}||_{\boxed{k}}$ is formulated as follows:

$$\parallel Z^{(v)} \parallel_{\boxed{k}} = \sum_{i=n-k+1}^{n} \lambda_i(L_{Z^{(v)}}) \tag{3}$$

where $\lambda_i(L_{Z^{(v)}})$ is the eigenvalues of $L_{Z^{(v)}}$ and $i \in [1\ n]$.

Problem and Motivation: Formula (2) necessitates that all perspectives of X are entirely comprehensive, a requirement that is impractical for IMVC tasks due to the varying sizes of graphs derived from incomplete perspectives. To tackle these challenges, some research endeavors concentrate on reconstructing the absent elements within the incomplete graphs linked to the missing perspectives [Lin *et al.*, 2021]. However, these endeavors typically entail significant computational expenses. Furthermore, achieving perfectly reconstructed graphs from incomplete multi-view data is unfeasible, which could potentially degrade clustering performance. Consequently, the optimal approach is to maximize the utilization of the information contained within the accessible instances from each view. By adopting the prior index information of the missing instances, we perform the following extension of $Z^{(v)}$:

$$\begin{aligned} &\min_{Z^{(v)},\bar{S}^{(v)}} \sum_{v=1}^{V} \parallel \bar{S}^{(v)} - {G^{(v)}}^T \tilde{Z}^{(v)} G^{(v)} \parallel_F^2 \\ &+ \sum_{v=1}^{V} \left(\beta \parallel X^{(v)} - X^{(v)}Z^{(v)} \parallel_1 + \gamma \parallel Z^{(v)} \parallel_{\boxed{k}} \right) \\ &s.t.\ diag(Z^{(v)}) = 0,\ Z^{(v)} \geq 0,\ Z^{(v)} = {Z^{(v)}}^T, \\ &0 \leq \bar{S}^{(v)} \leq 1,\ \bar{S}^{(v)} 1 = 1 \end{aligned} \tag{4}$$

where $G^{(v)}$ indicates the prior index information of the missing instances and $\bar{S}^{(v)}$ is the complete graph of the v-th view. Importantly, it can transform the incomplete graph with size $n_v \times n_v$ of each view to a full size affinity graph with size $n \times n$, such that the pairwise similarity relationships of instances between $\bar{S}$ and $Z^{(v)}$ can be alligned. In addition, $||\cdot||_1$ can better simulate noise and learning bias. Here, the high-confident local structure $\tilde{Z}^{(v)}$ is defined as follows:

$$\tilde{Z}_{i,j}^{(v)} = \begin{cases} q_{i,j}, & if\ x_i^{(v)}\ \&x_j^{(v)}\ \in\ \Psi(x_j^{(v)}) \\ 0, & otherwise \end{cases} \tag{5}$$

where $q_{i,j}$ indicates the distance between $x_i^{(v)}$ and $x_j^{(v)}$ calculated using the Gaussian kernel, and $\Psi(x_j^{(v)})$ presents the k block of instance $x_j^{(v)}$ on the v-th view. Otherwise, $G^{(v)}$ is computed as follows:

$$G_{i,j}^{(v)} = \begin{cases} 1, & if\ the\ i-th\ available\ instance\ x_i^{(v)} \\ & belongs\ to\ the\ j-th\ sample \\ 0, & otherwise \end{cases} \tag{6}$$

In particular, when dealing with incomplete multi-view data, the missing instances also result in the absence of certain pairwise correlations. Aiming to comprehensively exploit the complementary affinity information from different,

we further impose a high quality consensus graph to align the structures of all views. Thus, we propose the final efficient but simple objective function of HLSCG_IMC as follows:

$$\begin{aligned}\min_{Z^{(v)},S}&\sum_{v=1}^{V}\alpha_v^r \parallel (S-{G^{(v)}}^T\tilde{Z}^{(v)}G^{(v)})\odot W^{(v)} \parallel_F^2\\&+\sum_{v=1}^{V}\alpha_v^r\beta \parallel X^{(v)}-X^{(v)}Z^{(v)} \parallel_1\\&+\sum_{v=1}^{V}\alpha_v^r\gamma \parallel Z^{(v)} \parallel_{\boxed{k}}+\mu Tr(F^T L_S F)\\ s.t.\ &diag(Z^{(v)})=0,\ Z^{(v)}\geq 0,\ Z^{(v)}={Z^{(v)}}^T,\\&0\leq S\leq 1,\ S^{(v)}I=I,\ diag(S)=0\\&0\leq\alpha_v\leq 1,\ \sum_{v=1}^{V}\alpha=1\end{aligned} \tag{7}$$

where α_v denotes an adaptive learned weight, which is applied to jointly balance the importance of all views. Specifically, $F\in R^{n\times c}$ is the consensus representation, c is the manual selected dimension which is generally chosen as the cluster number. Besides this, L_S presents the Laplacian matrix of the complete structure $S\in R^{n\times n}$, which can be achieved by $L_S=DD^T-\frac{(S+S^T)}{2}$. In addition, $W^{(v)}$ can be calculated as follows:

$$W_{i,j}^{(v)}=\begin{cases}1, & if\ the\ i-th\ and\ j-th\ samples\\ & have\ instances\ on\ the\ v-th\ view\\0, & otherwise\end{cases} \tag{8}$$

where $W^{(v)}$ is the affinity relationship matrix between the missing instances and the existing instances.

3.2 Optimization

In this section, we use the alternating direction method of multipliers (ADMMs) to solve the optimization problem (7), which can be simply transformed into the following equivalent problem:

$$\begin{aligned}\min_{Z^{(v)},S}&\sum_{v=1}^{V}\alpha_v^r\Big(\parallel (S-\bar{Z}^{(v)})\odot W^{(v)} \parallel_F^2+\beta \parallel E^{(v)} \parallel_1\Big)\\&+\sum_{v=1}^{V}\alpha_v^r\gamma \parallel B^{(v)} \parallel_{\boxed{k}}+\frac{\lambda}{2}\sum_{i,j=1}^{n} \parallel F_{i,:}-F_{j,:} \parallel_2^2 S_{i,j}\\&+\sum_{v=1}^{V}\alpha_v^r\frac{\mu}{2} \parallel X^{(v)}-X^{(v)}Z^{(v)}-E^{(v)}+\frac{C_1^{(v)}}{\mu} \parallel_F^2\\&+\sum_{v=1}^{V}\alpha_v^r\frac{\mu}{2} \parallel Z^{(v)}-B^{(v)}+\frac{C_2^{(v)}}{\mu} \parallel_F^2\\ s.t.\ &diag(Z^{(v)})=0,\ Z^{(v)}\geq 0,\ Z^{(v)}={Z^{(v)}}^T,\ 0\leq S\leq 1,\\&S^{(v)}I=I,\ diag(S)=0,\ 0\leq\alpha_v\leq 1,\ \sum_{v=1}^{V}\alpha=1,\end{aligned} \tag{9}$$

where $C_1^{(v)}$ and $C_2^{(v)}$ are the imposed argumented variables, and $\bar{Z}^{(v)}={G^{(v)}}^T\tilde{Z}^{(v)}G^{(v)}$.

Solution of $Z^{(v)}$: With the other variables fixed, Z^v can be solved by optimizing the following formular:

$$\begin{aligned}\min_{Z^{(v)}}&\sum_{v=1}^{V}\alpha_v^r\Big(\frac{\mu}{2} \parallel X^{(v)}-X^{(v)}Z^{(v)}-E^{(v)}+\frac{C_1^{(v)}}{\mu} \parallel_F^2\\&+\frac{\mu}{2} \parallel Z^{(v)}-B^{(v)}+\frac{C_2^{(v)}}{\mu} \parallel_F^2\Big)\\ s.t.\ &diag(Z^{(v)})=0,\ Z^{(v)}\geq 0,\ Z^{(v)}={Z^{(v)}}^T\end{aligned} \tag{10}$$

Then, $Z^{(v)}$ can be calculated by setting the derivative of (10) with respect to $Z^{(v)}$ as 0:

$$Z^{(v)}=({X^{(v)}}^T X^{(v)}+2I)^{-1}({X^{(v)}}^T L_1^{(v)}+L_2^{(v)}) \tag{11}$$

where $L_1^{(v)}=X^{(v)}-E^{(v)}+\frac{C_1^{(v)}}{\mu}$ and $L_2^{(v)}=B^{(v)}-\frac{C_2^{(v)}}{\mu}$, respectively.

Solution of $B^{(v)}$: With the other variables fixed, $B^{(v)}$ can be solved by optimizing the following formular:

$$\begin{aligned}&\sum_{v=1}^{V}\alpha_v^r\left(\gamma \parallel B^{(v)} \parallel_{\boxed{k}}+\frac{\mu}{2} \parallel Z^{(v)}-B^{(v)}+\frac{C_2^v}{\mu} \parallel_F^2\right)\\ &s.t.\ diag(B^{(v)})=0,\ B^{(v)}\leq 0,\ B^{(v)}={B^{(v)}}^T\end{aligned} \tag{12}$$

Then, (18) can be simplified as follows:

$$\begin{aligned}&\sum_{v=1}^{V}\alpha_v^r\Big(\frac{\mu}{2} \parallel L_3^{(v)}-B^{(v)} \parallel_F^2\\&\qquad+\gamma<Diag(B^{(v)}\mathbf{1})-B^{(v)},\omega^{(v)}>\Big)\\ &s.t.\ diag(B^{(v)})=0,\ B^{(v)}\leq 0,\ B^{(v)}={B^{(v)}}^T\end{aligned} \tag{13}$$

where $L_3^{(v)}=Z^{(v)}+C_2^{(v)}/\mu$. Particularly, $\omega^{(v)}=U^{(v)}{U^{(v)}}^T$, where $U^{(v)}$ consists of k eigenvectors associated with the k smallest eigenvalues of $Diag(B^{(v)}\mathbf{1})-B^{(v)}$. Then, (19) can be rewritten as follows:

$$\begin{aligned}&\parallel B^{(v)}-L_3^{(v)}+\frac{\mu}{\gamma}(diag(\omega^{(v)})\mathbf{1}^T-\omega^{(v)}) \parallel_F^2\\ &s.t.\ diag(B^{(v)})=0,\ B^{(v)}\leq 0,\ B^{(v)}={B^{(v)}}^T\end{aligned} \tag{14}$$

This problem has a closed form solution given as follows:

$$\begin{aligned}&\parallel B^{(v)}-A^{(v)} \parallel_F^2\\ &s.t.\ diag(B^{(v)})=0,\ B^{(v)}\leq 0,\ B^{(v)}={B^{(v)}}^T\end{aligned} \tag{15}$$

where $A^{(v)}=L_3^{(v)}+\frac{\mu}{\beta}(diag(W^{(v)})\mathbf{1}^T-W^{(v)})$. Afterwards, $B^{(v)}$ can be updated as $B^{(v)}=(\hat{A^{(v)}}+\hat{A^{(v)}}^T)/2$, where $\hat{A^{(v)}}=A^{(v)}-Diag(diag(A^{(v)}))$.

Solution of $E^{(v)}$: With the other variables fixed, $E^{(v)}$ can be solved by optimizing the following formular:

$$\sum_{v=1}^{V}\alpha_v^r\Big(\beta \parallel E^{(v)} \parallel_1+\frac{\mu}{2} \parallel L_4^{(v)}-E^{(v)} \parallel_F^2\Big) \tag{16}$$

where $L_4^{(v)} = X^{(v)} - X^{(v)}Z^{(v)} + \frac{C_1^{(v)}}{\mu}$. Here, $E^{(v)}$ has the closed solution as follows:

$$E^{(v)} = \Omega_{\beta/\mu}(L_4^{(v)}) \tag{17}$$

where ω denotes the shrinkage operator.

Solution of S: With the other variables fixed, S can be solved by optimizing the following formular:

$$\begin{aligned}\sum_{v=1}^{V} \alpha_v^r \parallel (S - \bar{Z}^{(v)}) \odot W^{(v)} \parallel_F^2 \\ + \frac{\lambda}{2} \sum_{i,j=1}^{n} \parallel F_{i,:} - F_{j,:} \parallel_2^2 S_{i,j}\end{aligned} \tag{18}$$

By defining $H_{i,j} = \parallel F_{i,:} - F_{j,:} \parallel_2^2$, we can rewrite (18) as the following n independent sub-optimization problems with respect to each column of S:

$$\min_{S_{:,j}} \sum_{i=1}^{n} (S_{i,j} - \frac{\sum_{v=1}^{V} \alpha_v^r {W_{i,j}^{(v)}}^2 \bar{Z}_{i,j} - \frac{\lambda}{4} E_{i,j}}{\sum_{v=1}^{V} \alpha_v^r {W_{i,j}^{(v)}}^2})^2 \tag{19}$$

According to the Lagrangian algorithm, we can obtain the following closed form solution:

$$S_{i,j} = \begin{cases} (T_{i,j} + \delta_j)_+, & i \neq j \\ 0 \quad , & i = j \end{cases} \tag{20}$$

where $T_{i,j} = \frac{\sum_{v=1}^{V} \alpha_v^r {W_{i,j}^{(v)}}^2 \bar{Z}_{i,j} - \frac{\lambda}{4} E_{i,j}}{\sum_{v=1}^{V} \alpha_v^r {W_{i,j}^{(v)}}^2}$. Here, $(b)_+$ guarantees the non-negative value of b. Then, we can update $\delta_j = \frac{1 - \sum_{i=1, i \neq j}^{n} T_{i,j}}{n-1}$.

Solution of α: With the other variables fixed, α can be solved by optimizing the following formular:

$$\min_{\alpha_v} \sum_{v=1}^{V} \alpha_v^r d^{(v)} \; s.t. \; 0 \leq \alpha_v \leq 1, \; \sum_{v=1}^{V} \alpha = 1 \tag{21}$$

where $d^{(v)} = \parallel (S - \bar{Z}^{(v)}) \odot W^{(v)} \parallel_F^2 + \beta \parallel E^{(v)} \parallel_1 + gamma \parallel B^{(v)} \parallel_{\boxed{k}} + \frac{\mu}{2} \parallel X^{(v)} - X^{(v)}Z^{(v)} - E^{(v)} + \frac{C_1^{(v)}}{\mu} \parallel_F^2 + \frac{\mu}{2} \parallel Z^{(v)} - B^{(v)} + \frac{C_2^{(v)}}{\mu} \parallel_F^2$.

By imposing the Lagrange multiplier $sigma$, we can rewrite the optimization problem (21) as follows:

$$\sum_{v=1}^{V} \alpha_v^r d^{(v)} - \sigma(\sum_{v=1}^{V} \alpha_v^r - 1) \tag{22}$$

Then, we can update α by setting the derivative of (22) with respect to α_v as 0 as follows:

$$\alpha_v = (d^{(v)} / \sum_{v=1}^{V} d^{(v)})^{\frac{1}{1-r}}. \tag{23}$$

Solution of F: With the other variables fixed, F can be solved by optimizing the following formular:

$$\min_{F^T F} Tr(F^T L_S F) \tag{24}$$

Algorithm 1 Solution of HLSCG_IMC

Input: Incomplete multi-view data $\{X^{(v)} \in R^{d_v \times n_v}\}_{v=1}^{V}$, prior index matrix $G^{(v)}$, and parameters λ, β, and γ.
Initialization: Initialize $Z^{(v)}$ via the k-nearest neighbor graph of each view; Initialize F with the eigenvalue decomposition on the Laplacian graph of each transformed complete view; $C_1^{(v)} = 0$, $C_2^{(v)} = 0$; $C_3^{(v)} = 0$; $\mu = 0.1$.
Output: $Z^{(v)}$, F.

while iteration $< R$ **do**
  Update $Z^{(v)}$ using (11)
  Update $B^{(v)}$ using (15)
  Update $E^{(v)}$ using (17)
  Update S using (20)
  Update α using (23)
  Update F using (24)
  Update $C_1^{(v)}$ and $C_2^{(v)}$ using (25) and (26), respectively.
end while

Here, F can be gained as $F = [e_1, e_2, ..., e_c] \in R^{n \times c}$, where $e_1 \leq e_2 \leq ... \leq e_c$ are the c eigenvectors corresponding to the c minimum eigenvalues.

Solution of $C_1^{(v)}$ and $C_2^{(v)}$: With the other variables fixed, $C_1^{(v)}$ and $C_2^{(v)}$ can be solved by optimizing the following formulars:

$$C_1^{(v)} = C_1^{(v)} + \mu(X^{(v)} - X^{(v)}Z^{(v)} - E^{(v)}) \tag{25}$$

$$C_2^{(v)} = C_2^{(v)} + \mu(Z^{(v)} - B^{(v)}) \tag{26}$$

We present the detailed solutions for each variable of (9) in Algorithm 1.

3.3 Computation Complexity Analysis

In this sub-section, we make computation complexity analysis on the optimization steps of the proposed objective function. Firstly, for the step of $Z^{(v)}$, the most computational costs is the inverse operation calculated as n^3. Afterwards, ror the optimization approach of S and $B^{(v)}$, it is observable that the updating formula for the pertinent variable merely involves element-wise multiplication and division operations on matrices and vectors. Afterwards, the computational complexity of $E^{(v)}$ can be ignored since it only contains the basic matrix operations. For the solution of F, an efficient eigenvalue decomposition algorithm with the package 'eigs' serves as an excellent option, necessitating only $O(cn^2)$ operations to obtain the optimal F. Finally, for the step of α, its updating formula similarly encompasses solely element-wise division operations for vectors. Consequently, the total computational cost of the proposed objective function is $O(\tau(cn^2 + n^3))$, where tau denotes the number of interations.

Data	Methods	ACC (%)			NMI (%)			Purity (%)		
		0.1	0.3	0.5	0.1	0.3	0.5	0.1	0.3	0.5
BBCSport	BSV	58.62±3.94	51.31±5.33	44.03±3.98	43.73±7.43	31.03±2.08	21.40±2.61	65.79±5.52	55.07±1.51	47.59±2.28
	Concat	70.62±3.76	58.72±5.42	33.21±2.19	61.69±6.72	38.92±7.87	18.61±1.44	80.59±4.59	63.24±5.82	37.00±1.54
	GPMVC	51.44±8.20	46.89±5.01	43.91±6.31	28.23±10.31	20.04±7.39	15.48±4.54	58.39±8.58	52.76±5.60	45.29±5.41
	MIC	51.21±4.21	46.21±4.71	46.03±5.19	29.90±6.25	25.84±3.24	24.01±5.39	55.00±4.15	51.72±4.27	52.41±6.23
	DAIMC	68.62±4.59	63.45±10.97	56.89±5.59	56.62±4.60	50.17±9.91	37.89±6.22	76.90±5.89	71.72±10.76	61.03±5.08
	OMVC	53.33±3.21	51.38±3.06	48.79±3.10	30.64±2.00	41.57±2.79	40.63±2.45	56.49±2.81	59.20±2.12	57.47±2.80
	MVL_IV	75.86±2.28	72.58±0.50	53.45±1.49	60.55±4.42	59.09±5.05	38.85±1.36	81.03±3.48	80.75±1.32	62.93±1.49
	AWIMVC	77.61±2.01	78.33±2.25	64.75±2.69	71.01±2.79	69.51±2.17	49.48±2.03	86.44±1.30	85.42±0.97	73.55±1.20
	UEAF	75.52±3.59	68.62±5.87	62.93±5.69	67.38±1.56	58.43±3.57	46.51±4.52	85.34±1.72	78.28±3.83	71.03±3.48
	AGC_IMVC	83.10±5.74	80.17±3.19	70.86±6.14	73.19±4.73	67.79±4.88	52.41±5.92	86.03±2.08	83.79±3.83	76.03±4.54
	Proposed	**85.34±0.15**	**82.17±1.11**	**78.48±0.28**	**76.53±2.01**	**70.22±1.42**	**62.66±1.00**	**95.93±1.06**	**88.73±1.36**	**83.09±0.46**
COIL-20	BSV	41.46±6.90	40.42±3.48	35.97±4.55	53.38±5.57	51.22±4.40	43.08±6.90	46.07±4.66	43.68±2.58	38.42±6.90
	Concat	31.35±2.43	28.89±8.62	22.64±3.83	45.58±1.47	42.34±7.49	35.20±2.28	33.62±2.17	31.11±3.67	24.38±1.99
	GPMVC	38.43±2.89	40.00±8.80	34.72±7.00	49.17±3.37	50.35±3.88	42.72±4.35	40.50±9.90	41.88±4.90	38.12±6.65
	MIC	40.15±4.84	42.63±1.99	32.17±5.86	48.95±8.82	51.33±8.23	46.10±4.61	43.28±7.32	40.10±1.79	39.17±2.07
	DAIMC	84.15±3.11	83.68±1.99	76.25±2.07	83.15±4.41	82.33±1.03	78.46±2.06	86.33±5.71	86.87±8.62	79.24±9.85
	OMVC	49.38±4.35	46.53±3.46	50.19±5.62	61.07±3.13	62.64±1.98	59.51±2.55	54.11±4.32	49.03±2.89	55.40±3.76
	MVL_IV	50.13±0.92	48.54±1.64	52.43±1.15	63.59±1.54	62.81±0.99	63.28±0.85	53.37±3.83	52.78±1.60	56.53±1.21
	AWIMVC	51.02±0.99	46.55±0.71	33.49±1.77	56.90±0.43	50.71±1.90	54.30±1.32	55.21±1.68	41.70±1.61	33.59±1.52
	UEAF	53.66±4.61	47.22±6.20	36.04±3.68	59.88±6.09	52.31±5.96	44.46±6.14	54.37±3.88	48.82±4.91	38.89±8.43
	AGC_IMVC	84.12±1.04	83.54±2.41	76.18±3.96	82.68±0.79	82.22±1.04	80.59±5.55	87.35±2.04	86.94±1.41	79.17±3.77
	Proposed	**89.17±0.47**	**84.88±1.15**	**84.30±1.05**	**87.36±0.88**	**84.55±2.04**	**82.01±0.78**	**87.40±1.37**	**88.72±2.06**	**83.71±1.12**
Caltech-7	BSV	43.89±1.37	39.06±1.26	38.31±1.68	39.66±2.23	31.63±1.51	26.81±1.38	84.08±1.23	75.25±0.71	68.97±0.49
	Concat	41.25±1.67	40.55±1.89	38.06±0.88	43.48±0.92	37.99±2.17	30.28±0.66	84.91±0.50	82.54±1.12	77.56±0.98
	GPMVC	38.43±2.89	40.00±8.80	34.72±7.00	49.17±3.37	50.35±3.88	42.72±4.35	40.50±9.90	41.88±4.90	38.12±6.65
	MIC	44.07±4.97	38.01±2.12	35.80±2.34	33.71±2.66	27.35±1.69	20.44±0.98	78.12±1.76	73.31±0.72	68.26±1.40
	DAIMC	48.29±6.76	47.46±3.42	44.89±4.88	44.61±3.88	38.45±2.88	36.28±2.34	83.32±1.31	76.83±3.23	75.50±1.17
	OMVC	49.38±4.35	46.53±3.46	50.19±5.62	61.07±3.13	62.64±1.98	59.51±2.55	54.11±4.32	49.03±2.89	55.40±3.76
	MVL_IV	50.13±0.92	48.54±1.64	52.43±1.15	63.59±1.54	62.81±0.99	63.28±0.85	53.37±3.83	52.78±1.60	56.53±1.21
	AWIMVC	51.02±0.99	46.55±0.71	33.49±1.77	56.90±0.43	50.71±1.90	44.30±1.32	55.21±1.68	41.70±1.61	33.59±1.52
	UEAF	50.82±4.05	42.71±0.84	36.32±4.22	39.44±2.07	31.07±1.99	24.02±1.37	81.49±1.78	78.26±2.12	76.29±1.93
	AGC_IMVC	59.63±4.11	57.31±2.13	55.10±2.66	59.68±2.55	59.47±1.28	59.37±2.36	84.14±2.24	61.59±2.01	60.22±2.57
	Proposed	**64.86±1.19**	**83.92±0.32**	**65.67±2.04**	**65.95±1.15**	**68.35±2.40**	**69.29±0.11**	**87.31±0.37**	**86.66±0.49**	**84.46±2.15**
BUAA	BSV	33.64±6.15	30.02±10.03	26.59±2.71	56.22±3.45	54.29±8.62	46.47±6.14	32.17±5.50	31.62±6.69	28.22±9.78
	Concat	28.43±9.77	26.07±4.02	23.56±8.61	63.61±6.13	60.59±2.07	55.95±7.15	29.88±5.41	27.71±7.40	24.74±8.58
	GPMVC	34.57±8.52	32.29±5.03	27.19±4.74	57.18±9.95	55.34±7.21	47.24±4.97	35.40±5.74	33.63±2.70	28.52±3.48
	MIC	35.63±5.31	34.77±4.97	29.16±3.13	59.65±2.07	55.42±6.07	46.20±3.66	37.10±4.56	36.33±3.10	29.16±3.94
	DAIMC	29.11±1.08	27.41±3.10	25.63±5.31	56.85±3.68	54.39±2.17	57.64±8.62	30.01±5.81	28.74±6.20	26.81±6.69
	OMVC	43.57±7.48	30.61±6.03	28.77±2.23	63.59±2.07	62.17±3.89	54.91±4.39	46.48±5.33	40.10±5.05	37.11±7.18
	MLV_IV	44.07±3.72	36.81±1.16	31.11±0.27	72.00±1.35	66.83±2.53	62.63±0.14	45.48±0.95	38.16±1.01	32.74±0.41
	AWIMVC	47.11±1.50	41.02±1.67	33.27±0.68	72.55±1.66	62.09±1.05	61.22±0.93	48.47±0.89	43.68±0.48	36.49±0.74
	UEAF	35.93±4.30	30.59±3.97	26.74±9.66	66.64±5.27	60.46±7.94	59.14±3.38	37.56±5.20	32.22±4.41	28.07±3.97
	AGC_IMVC	37.26±4.68	26.74±0.67	25.48±2.70	61.51±5.05	53.87±0.61	57.51±5.25	38.96±1.66	28.01±1.37	26.67±3.72
	Proposed	**58.74±0.88**	**51.26±1.03**	**48.26±1.27**	**73.83±0.65**	**68.48±0.87**	**64.15±1.09**	**52.44±1.24**	**73.37±0.41**	**56.37±2.52**

Table 2: ACC (%), NMI (%), and Purity (%) of different methods on the BBCSport, COIL-20, Caltech-7, and BUAA datasets, respectively.

4 Experiments and Analysis

4.1 Database Description

BBCSport[1]**:** BBCSport constitutes a document database comprising 737 news articles pertaining to five sports: athletics, cricket, football, rugby, and tennis, sourced from the BBC Sport website between 2004 and 2005. For the purpose of evaluating various algorithms grounded in Integrated Multi-view Clustering (IMC), a subset from the BBC sport multi-view datasets, encompassing four distinct views, was utilized. This specific subset contains 116 samples, where each of the four views possesses a feature dimensionality of 1991, 2063, 2113, and 2158, respectively. **The Columbia Object Image Library**[2] (COIL-20) comprises a total of 1,440 images spread across 20 different classes. To create the multi-view dataset, we extracted three feature types from each image: deep features using the VGG-F model [Zhao *et al.*, 2019], Local Binary Patterns (LBP) features [Oliva and Torralba, 2001], and vectored pixel features. Meanwhile, the Caltech101 database encompasses 101 object categories, with each class having between 40 to 800 images [Fei-Fei *et al.*, 2004]. For the comparison experiments conducted in this paper, a subset known as Caltech-7 was chosen, which includes 1474 images from 7 classes. Specifically, the selected multi-view dataset for Caltech-7 consists of two views: GIST and LBP features [Li *et al.*, 2015]. Referring to [Zhao *et al.*, 2016], a subset of the **BUAA-visnir face database** [3] was chosen to evaluate the proposed method, which comprises two views, i.e., 90 visual images and 90 near-infrared images, all belonging to the first 10 classes.

Incomplete multi-view data construction: In this paper, the incomplete multi-view dataset was created by randomly removing 10%, 30%, and 50% instances in each view. Then, every algorithm method was carried out on each dataset 10 times, and the average value was reported as the final result. The evaluation metrics used were clustering accuracy (ACC), normalized mutual information (NMI), and purity [Wen *et al.*,

[1]https://github.com/GPMVCDummy/GPMVC/tree/master/partialMV/PVC/recreateResults/data

[2]http://www.cs.columbia.edu/CAVE/software/softlib/coil-20.php

[3]https://github.com/hdzhao/IMG/tree/master/data.

2020]. All experiments conducted in this study were run on MATLAB R2020a, utilizing a hardware setup with 16.0 GB of RAM and a 3.40 GHz CPU.

4.2 Experimental Results and Analysis

In the comparative experiments, the proposed method was evaluated alongside a range of state-of-the-art IMC methods., i.e., BSV [Zhao *et al.*, 2016], Concat [Zhao *et al.*, 2016], GP-MVC [Rai *et al.*, 2016], MIC [Shao *et al.*, 2015], DAIMC [Hu and Chen, 2019], OMVC [Shao *et al.*, 2016], MVL_IV [Xu *et al.*, 2015], AWIMVC [Deng *et al.*, 2020], UEAF [Wen *et al.*, 2019], and AGC_IMVC [Wen *et al.*, 2020]. Table 2 reports the experimental results on the BBCSport, COLI-20, Caltech-7, and BUAA databases, respectively. From Table 2, it can be observed that:

(1) The proposed method can always obtainsthe best clustering performances on different incomplete multi-view databases. It shows that graph-based methods have clear advantages compared to the other related methods.

(2) Because the proposed method is capable of uncovering higher-order correlations among various views, it outperforms the other methods in terms of performance.

(3) The proposed method can be flexibly adopted to various types of IMC tasks.

4.3 Parameter Sensitivity Analysis

Three parameters, namely λ, β, and γ, are required to be adjusted for the proposed objective function. To identify the optimal parameter combination for each database, a series of experiments were conducted on the BUAA dataset. Figure 2 illustrates the sensitivity of the proposed method on different combinations of parameters on the BUAA dataset. Notably, our method exhibits minimal sensitivity to λ within the range of $[10^{-3}, 1]$. Furthermore, it is evident that the highest clustering accuracy for the BUAA database is achieved with β and γ in the range of $[10^{-5}, 1]$ and $[10^{-5}, 1]$, respectively.

4.4 Ablation Experiments

To demonstrate the effectiveness of the block diagonal structure embedding term, we implemented a variation that utilized a traditional K-NN to construct the affinity graph. This variation was evaluated on the COIL-20 and Caltech-101 databases, each with a 30% missing rate of views. Figure 3 depicts the experimental results of the proposed method incorporating different activation components. It can be obviously observed from Figure 3 that the proposed strategy consistently achieve the highest clustering accuracies.

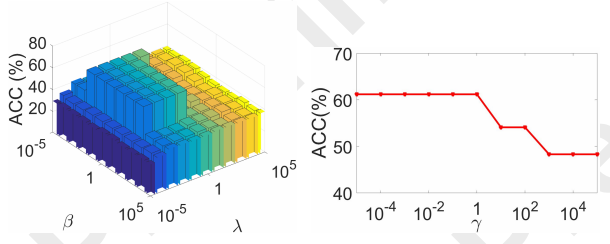

Figure 2: Clustering accuracies (ACC) versus different combinations of parameters on the BUAA dataset.

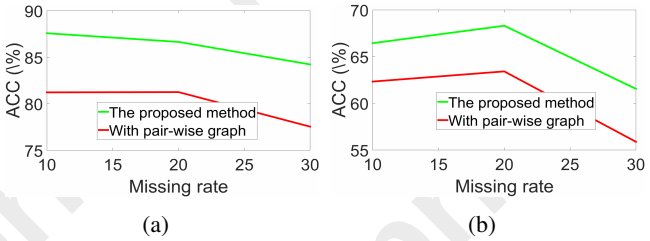

Figure 3: Comparison of the proposed method with different activation components on the (a) COIL-20 and (b) Caltech-101 databases with 30% missing rate of views, respectively.

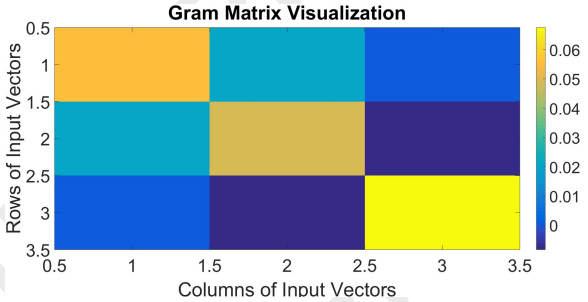

Figure 4: Gram visualization of the proposed method on the BBCSport dataset.

4.5 Visualization

In this subsection, we applied the widely used Gram matrix visualization algorithm to the BBCSport dataset, which has a 10% missing rate in each view. This algorithm utilizes a color scale to depict the magnitude of the values within the matrix, with darker shades representing higher values and brighter shades indicating lower values. As illustrated in Figure 4, it is evident that our proposed method effectively recovers the ground-truth diagonal block structure, where each diagonal block corresponds to a distinct cluster.

5 Conclusions

In this paper, a novel and efficient IMC framework, called HLSCG_IMC, for incomplete multi-view clustering is proposed. Unliking the other related works, it considers the attribution of instances with weak feature representation located at the edge of two clusters. Afterwards, a high-confident local structure is learned for each view to guide the intrinsic and complete structure construction. The experimental results demonstrate that the proposed method can effectively recover the missing affinity relationships and notably enhance the performance of IMVC. In the future, HLSCG_IMC will be adopted to more application scenarios.

Acknowledgments

This work was partially supported by the Guangdong Basic and Applied Basic Research Foundation (Grant no. 2024A1515011647, and 2024A1515030213), and the Shenzhen Fundamental Research Program (Grant no. Ref.JCYJJCYJ20240813154703005).

References

[Cai *et al.*, 2024] Yiran Cai, Hangjun Che, Baicheng Pan, Man-Fai Leung, Cheng Liu, and Shiping Wen. Projected cross-view learning for unbalanced incomplete multi-view clustering. *Information Fusion*, 105:102245, 2024.

[Chao *et al.*, 2024] Guoqing Chao, Yi Jiang, and Dianhui Chu. Incomplete contrastive multi-view clustering with high-confidence guiding. In *Proceedings of the AAAI Conference on Artificial Intelligence*, volume 38, pages 11221–11229, 2024.

[Chen *et al.*, 2024] Jie Chen, Yingke Chen, Zhu Wang, Haixian Zhang, and Xi Peng. Spectral embedding fusion for incomplete multiview clustering. *IEEE Transactions on Image Processing*, 33:4116–4130, 2024.

[Deng *et al.*, 2020] Wanyu Deng, Lixia Liu, Jianqiang Li, and Yijun Lin. Auto-weighted incomplete multi-view clustering. *IEEE Access*, 8:138752–138762, 2020.

[Fei-Fei *et al.*, 2004] Li Fei-Fei, Rob Fergus, and Pietro Perona. Learning generative visual models from few training examples: An incremental bayesian approach tested on 101 object categories. In *2004 conference on computer vision and pattern recognition workshop*, pages 178–178. IEEE, 2004.

[Fu *et al.*, 2024] Lele Fu, Sheng Huang, Lei Zhang, Jinghua Yang, Zibin Zheng, Chuanfu Zhang, and Chuan Chen. Subspace-contrastive multi-view clustering. *ACM Transactions on Knowledge Discovery from Data*, 18(9):1–35, 2024.

[Gu *et al.*, 2024] Zhibin Gu, Zhendong Li, and Songhe Feng. Topology-driven multi-view clustering via tensorial refined sigmoid rank minimization. In *Proceedings of the 30th ACM SIGKDD Conference on Knowledge Discovery and Data Mining*, pages 920–931, 2024.

[Hu and Chen, 2019] Menglei Hu and Songcan Chen. Doubly aligned incomplete multi-view clustering. *arXiv preprint arXiv:1903.02785*, 2019.

[Jiang *et al.*, 2025] Kun Jiang, Zhihai Yang, and Qindong Sun. Self-weighted subspace clustering via adaptive rank constrained graph embedding. *Pattern Analysis and Applications*, 28(1):23, 2025.

[Khan *et al.*, 2024] Ghufran Ahmad Khan, Jalaluddin Khan, Taushif Anwar, Zubair Ashraf, Mohammad Hafeez Javed, and Bassoma Diallo. Weighted concept factorization based incomplete multi-view clustering. *IEEE Transactions on Artificial Intelligence*, 5(11):5699–5708, 2024.

[Li *et al.*, 2015] Yeqing Li, Feiping Nie, Heng Huang, and Junzhou Huang. Large-scale multi-view spectral clustering via bipartite graph. In *Twenty-ninth AAAI conference on artificial intelligence*, 2015.

[Lin *et al.*, 2021] Yijie Lin, Yuanbiao Gou, Zitao Liu, Boyun Li, Jiancheng Lv, and Xi Peng. Completer: Incomplete multi-view clustering via contrastive prediction. In *Proceedings of the IEEE/CVF conference on computer vision and pattern recognition*, pages 11174–11183, 2021.

[Liu *et al.*, 2023a] Cheng Liu, Si Wu, Rui Li, Dazhi Jiang, and Hau-San Wong. Self-supervised graph completion for incomplete multi-view clustering. *IEEE Transactions on Knowledge and Data Engineering*, 35(9):9394–9406, 2023.

[Liu *et al.*, 2023b] Maoshan Liu, Yan Wang, Vasile Palade, and Zhicheng Ji. Multi-view subspace clustering network with block diagonal and diverse representation. *Information Sciences*, 626:149–165, 2023.

[Lu *et al.*, 2018] Canyi Lu, Jiashi Feng, Zhouchen Lin, Tao Mei, and Shuicheng Yan. Subspace clustering by block diagonal representation. *IEEE transactions on pattern analysis and machine intelligence*, 41(2):487–501, 2018.

[Lyu *et al.*, 2024] Gengyu Lyu, Weiqi Kang, Haobo Wang, Zheng Li, Zhen Yang, and Songhe Feng. Common-individual semantic fusion for multi-view multi-label learning. In *International Joint Conference on Artificial Intelligence*, pages 4715–4723, 2024.

[Oliva and Torralba, 2001] Aude Oliva and Antonio Torralba. Modeling the shape of the scene: A holistic representation of the spatial envelope. *International journal of computer vision*, 42(3):145–175, 2001.

[Rai *et al.*, 2016] Nishant Rai, Sumit Negi, Santanu Chaudhury, and Om Deshmukh. Partial multi-view clustering using graph regularized nmf. In *2016 23rd International Conference on Pattern Recognition (ICPR)*, pages 2192–2197. IEEE, 2016.

[Shao *et al.*, 2015] Weixiang Shao, Lifang He, and Philip S Yu. Multiple incomplete views clustering via weighted nonnegative matrix factorization with $l_{2,1}$ regularization. In *Joint European conference on machine learning and knowledge discovery in databases*, pages 318–334. Springer, 2015.

[Shao *et al.*, 2016] Weixiang Shao, Lifang He, Chun-ta Lu, and S Yu Philip. Online multi-view clustering with incomplete views. In *2016 IEEE International conference on big data (Big Data)*, pages 1012–1017. IEEE, 2016.

[Sun *et al.*, 2024] Yuan Sun, Yang Qin, Yongxiang Li, Dezhong Peng, Xi Peng, and Peng Hu. Robust multi-view clustering with noisy correspondence. *IEEE Transactions on Knowledge and Data Engineering*, 36(12):9150–9162, 2024.

[Wang *et al.*, 2022] Siwei Wang, Xinwang Liu, Li Liu, Wenxuan Tu, Xinzhong Zhu, Jiyuan Liu, Sihang Zhou, and En Zhu. Highly-efficient incomplete large-scale multi-view clustering with consensus bipartite graph. In *Proceedings of the IEEE/CVF conference on computer vision and pattern recognition*, pages 9776–9785, 2022.

[Wang *et al.*, 2023] Jing Wang, Songhe Feng, Gengyu Lyu, and Zhibin Gu. Triple-granularity contrastive learning for deep multi-view subspace clustering. In *Proceedings of the 31st ACM international conference on multimedia*, pages 2994–3002, 2023.

[Wen *et al.*, 2019] Jie Wen, Zheng Zhang, Yong Xu, Bob Zhang, Lunke Fei, and Hong Liu. Unified embedding

alignment with missing views inferring for incomplete multi-view clustering. In *Proceedings of the AAAI conference on artificial intelligence*, volume 33, pages 5393–5400, 2019.

[Wen *et al.*, 2020] Jie Wen, Ke Yan, Zheng Zhang, Yong Xu, Junqian Wang, Lunke Fei, and Bob Zhang. Adaptive graph completion based incomplete multi-view clustering. *IEEE Transactions on Multimedia*, 23:2493–2504, 2020.

[Wen *et al.*, 2021] Jie Wen, Zhihao Wu, Zheng Zhang, Lunke Fei, Bob Zhang, and Yong Xu. Structural deep incomplete multi-view clustering network. In *Proceedings of the 30th ACM international conference on information & knowledge management*, pages 3538–3542, 2021.

[Xu *et al.*, 2015] Chang Xu, Dacheng Tao, and Chao Xu. Multi-view learning with incomplete views. *IEEE Transactions on Image Processing*, 24(12):5812–5825, 2015.

[Yao *et al.*, 2024] Mingze Yao, Huibing Wang, Yawei Chen, and Xianping Fu. Between/within view information completing for tensorial incomplete multi-view clustering. *IEEE Transactions on Multimedia*, pages 1–13, 2024.

[Zhao *et al.*, 2016] Handong Zhao, Hongfu Liu, and Yun Fu. Incomplete multi-modal visual data grouping. In *IJCAI*, pages 2392–2398, 2016.

[Zhao *et al.*, 2019] Shuping Zhao, Bob Zhang, and CL Philip Chen. Joint deep convolutional feature representation for hyperspectral palmprint recognition. *Information Sciences*, 489:167–181, 2019.

[Zhong *et al.*, 2024] Qiyu Zhong, Gengyu Lyu, and Zhen Yang. Align while fusion: A generalized nonaligned multiview multilabel classification method. *IEEE Transactions on Neural Networks and Learning Systems*, 2024.

[Zhou *et al.*, 2019] Wei Zhou, Hao Wang, and Yan Yang. Consensus graph learning for incomplete multi-view clustering. In *Advances in Knowledge Discovery and Data Mining: 23rd Pacific-Asia Conference, PAKDD 2019, Macau, China, April 14-17, 2019, Proceedings, Part I 23*, pages 529–540. Springer, 2019.

[Zhuo *et al.*, 2024] Jiaming Zhuo, Can Cui, Kun Fu, Bingxin Niu, Dongxiao He, Chuan Wang, Yuanfang Guo, Zhen Wang, Xiaochun Cao, and Liang Yang. Graph contrastive learning reimagined: Exploring universality. In *Proceedings of the ACM on Web Conference 2024*, pages 641–651, 2024.